Instability of Interarea Oscillation Mode by Autoparametric Resonance

Naoto Kakimoto, *Member, IEEE*, Akira Nakanishi, and Katsuyuki Tomiyama

***Abstract*—There is a low-frequency interarea oscillation mode in middle and western 60-Hz areas of Japan. The mode is damped, i.e., stable for small disturbances, but diverges in an oscillatory manner for large disturbances. It restricts power transmission in the areas. This paper shows that the instability is caused by nonlinear interactions between a few modes. The areas are represented with West30-machine system model prepared by the IEE of Japan. Numerical simulations are executed to obtain a critical case in which generator swings last without diverging or damping. Natural oscillation modes contained in the swings, are then calculated. Two modes have strong interactions with the interarea mode, and act so as to deteriorate its damping. Last, we examine how their influence changes with load level of the system.**

***Index Terms*—Autoparametric resonance, interarea oscillation mode, power system stability.**

I. Introduction

MIDDLE and western 60-Hz areas of Japan form a typical longitudinal power system. A weakly damped interarea oscillation mode exists in the system, and restricts its transmission capacity. Eigenvalue analysis is effective for small disturbances. However, for large disturbances like three phase short circuits, nonlinear modal interaction becomes strong, and has significant effect on the stability [1]–[4].

Autoparametric resonance is a phenomenon in which one oscillation mode is excited by other oscillation modes to grow [5]. Several studies have been made on power systems [1], [2], [6]–[9]. For the resonance to occur, mode frequencies must satisfy some relation. In longitudinal power systems, however, the ratio of the lowest frequency to the second one is about 1:2, and the autoparametric resonance occurs in a natural manner. Modal interaction is brought by loads. As loads increase in amount, the interaction becomes stronger. For this reason, most studies do not consider generator control systems. However, the resonance is observed in a system with automatic voltage regulators. Further, a Hopf bifurcation occurs due to excitation system dynamics in a single machine infinite bus system [10]. Some studies have been made on this phenomenon [11]–[13]. Its application to longitudinal power systems is being attempted.

This paper examines an autoparametric resonance in a power system named West30-machine system model. This model was prepared by the IEE of Japan, and it represents the middle and western areas of Japan. In this model, automatic voltage regulators and speed governors are considered, active load power is represented as constant current, and its structure is not simple but reflects the real system. In this analysis, generator swings are decomposed into natural oscillation modes, and their interaction is investigated. Harmonic balance method is applied to derive periodic solutions [14]. By this analysis, it is clarified that the 1:2 autoparametric resonance occurs in this model system. Further, 1:1 resonance with a mode related with the control systems appears. This resonance has been overlooked in the preceding studies. It may be related with the prescribed Hopf bifurcation. We observe how two modes interact to cause the resonance. The 1:2 and 1:1 resonances both act so as to make the interarea mode diverge. We examine their participation in the instability.

First, we describe the object system, and execute numerical simulations to see how generator swings diverge in Section II. Next, we do eigenvalue analysis to examine force which acts between modes in Section III. Further, we examine two resonances among modes in Section IV. Lastly, we show relation between load and critical clearing time, and then how each resonance participates in the instability in Section V. The results are summarized in Section VI.

Manuscript received April 19, 2004. Paper no. TPWRS-00583-2002.

N. Kakimoto is with Kyoto University, Kyoto, Japan (e-mail: kakimoto@kuee.kyoto-u.ac.jp).

A. Nakanishi is with Ito-chu Corporation, Tokyo, Japan.

K. Tomiyama is with Kansai Electric Power Company, Osaka, Japan.

Digital Object Identifier 10.1109/TPWRS.2004.836265

II. Description of Phenomenon

A. Power System

Fig. 1 shows the IEEJ West30-machine system. This system represents the middle and western 60-Hz areas of Japan. There are 30 generators, 115 buses, and 99 transmission lines. Total generation capacity is 128 840 MVA and load is 100 200 MW.

Each generator has a field winding and a damper winding in d-axis, and a damper winding in q-axis. Fig. 2 shows its excitation system, where V_t is terminal voltage, and E_{fd} is excitation voltage. There are two types of speed governors. One in Fig. 3(a) is used for 25 thermal or nuclear generators. One in Fig. 3(b) is used for five hydraulic generators, i.e., G_2, G_8, G_{14}, G_{24}, G_{25}. $\Delta\omega$ denotes rotor speed deviation, and P_m is mechanical input.

Loads depend nonlinearly on bus voltages. Active power is assumed to be constant current, and reactive power is constant impedance. Their frequency characteristics is not considered. As for system parameters, refer to http://www.iee.or.jp.

B. Swing Equations

Each generator has 13 or 11 state variables related with the rotor angle, speed, flux, excitation system, and speed governor. Total state variables are 380, denoted by n, for the system in Fig. 1. Their time variation is described by

$$\frac{du}{dt} = \varphi(u) \tag{1}$$

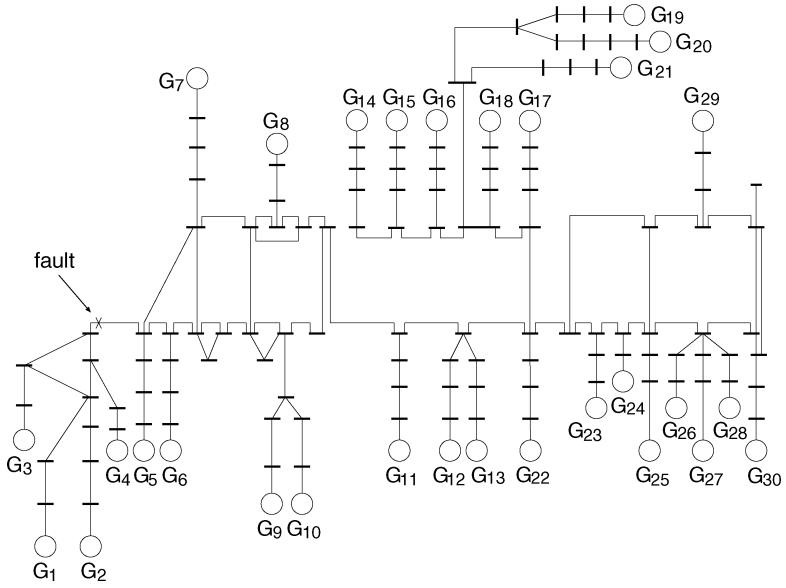

Fig. 1. IEEJ West30-machine system.

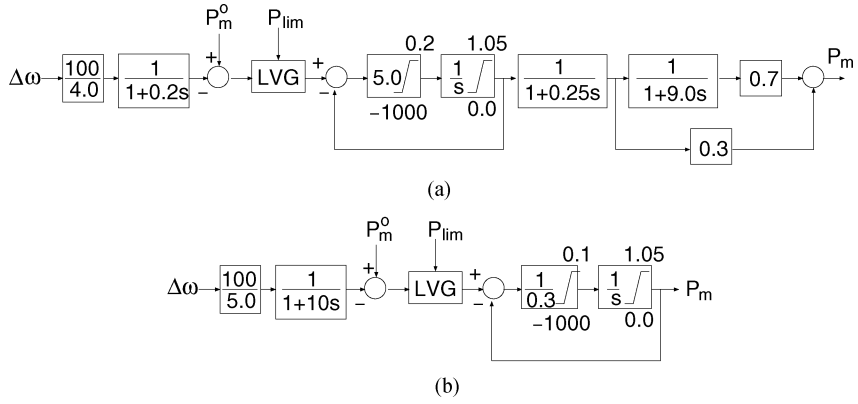

Fig. 3. Speed governor.

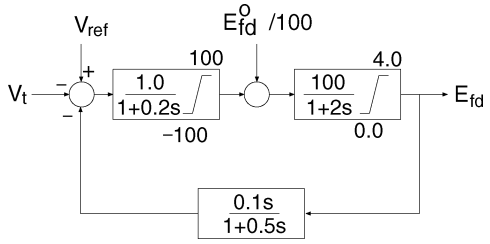

Fig. 2. Excitation system.

where u and φ are $n\times 1$ vectors. $\varphi(u_o) = 0$ holds at an initial equilibrium point u_o. We use the Runge-Kutta method for numerical solution of (1).

Fig. 4 shows swing curves for a three phase short circuit fault indicated in Fig. 1. Load level is 0.9; we multiply each load and generator power by 0.9. The system is returned to the initial one after clearance of the fault. G_{30} is a reference of rotor angle. If clearing time t_c is 0.110 s, rotor swings decay with time as in Fig. 4(a). Fig. 4(b) is for a critical clearing time of 0.114 s, in which the swings last. However, if the clearing time is 0.118 s, the swings diverge in an oscillatory manner, as shown in Fig. 4(c).

The critical clearing time for the first swing instability is 0.214 s. Compared with this value, 0.114 s for Fig. 4 is considerably small. This means that the instability observed in Fig. 4 is more important than the first swing instability. It is unknown why this phenomenon occurs. In the following, we clarify its mechanism.

III. Mode Analysis

A. Eigenvalue Analysis

Linearizing (1) at the equilibrium point u_o gives

$$\frac{dv}{dt} = Av \tag{2}$$

where A is an $n \times n$ matrix and

$$v \equiv u - u_o.$$

There are n eigenvalues in this system. A pair of conjugate eigenvalues denoted by

$$\lambda_i, \bar{\lambda}_i = d_i \pm j\omega_i \tag{3}$$

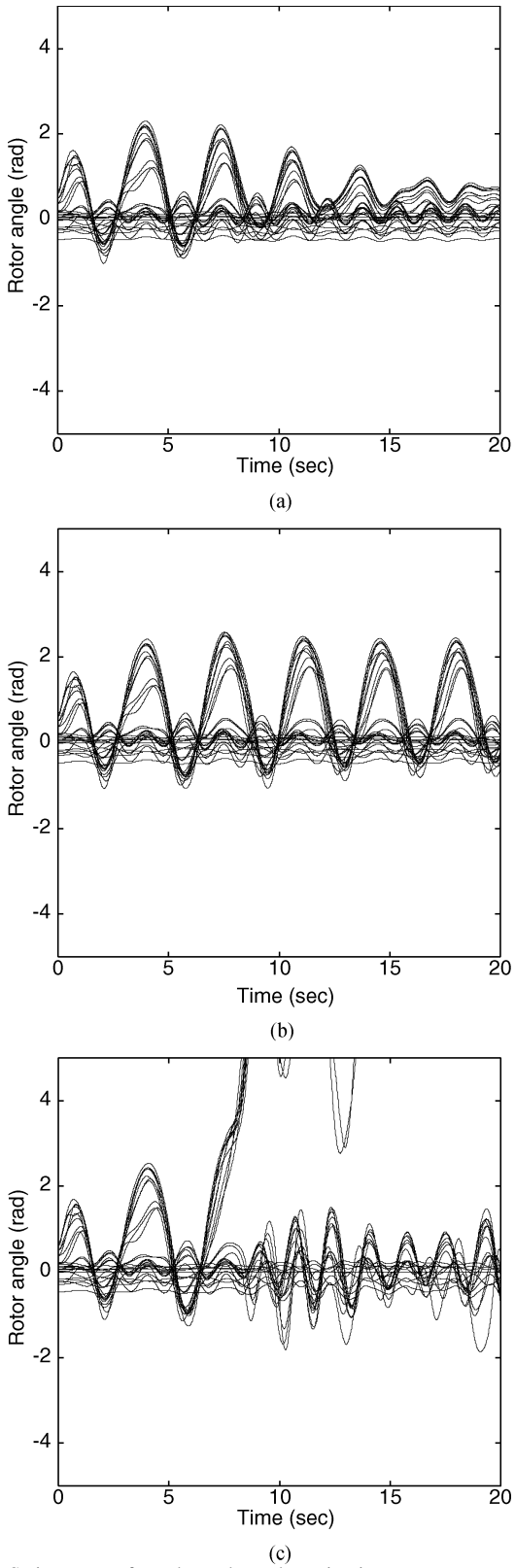

Fig. 4. Swing curves for a three phase short circuit.

correspond to a natural oscillation mode i. Important ones are

0: $-0.287 \pm j1.330$
1: $-0.164 \pm j2.272$
2: $-0.037 \pm j3.937$
3: $-0.044 \pm j4.159$

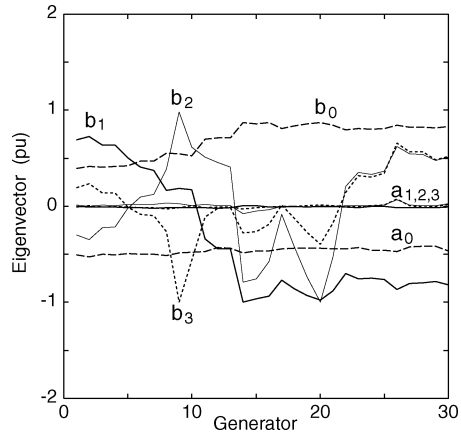

Fig. 5. Eigenvectors.

where $0 \sim 3$ are mode numbers. The eigenvectors corresponding to these eigenvalues are expressed by

$$\xi_i, \bar{\xi}_i = a_i \pm j b_i \tag{4}$$

where ξ_i, a_i, and b_i are $n \times 1$ vectors.

Fig. 5 shows parts of vector a_i and b_i for mode $0 \sim 3$. Only components corresponding to rotor angles are shown. $a_1 \sim a_3 \simeq 0$ for rotor angles. b_1 shows that generators $G_1 \sim G_{10}$ oscillate against the remaining generators in mode 1. We can see this mode clearly in Fig. 4(b).

B. Mode Component

Consider a linear transformation

$$v = Mz \tag{5}$$

where

$v \quad = u - u_o;$
$M \quad \equiv (a_0, b_0, a_1, b_1, \ldots);$
$z \quad \equiv (x_0, y_0, x_1, y_1, \ldots)^t.$

x_i and y_i are components corresponding to a_i and b_i. Two eigenvalues λ_i, $\bar{\lambda}_i$ correspond to a_i and b_i as in (4). If an eigenvalue λ_i is real number, only a_i and x_i are incorporated in M and z. Since there are n eigenvalues in all, M is $n \times n$ matrix, and z is $n \times 1$ vector. We assume M is nonsingular and diagonalizable.

Fig. 6 shows time variations of the component y_i for Fig. 4(b) which is obtained by solving (5). Mode $0 \sim 3$ have different natural frequencies, and they oscillate independently right after the fault. However, they synchronize soon, and oscillate periodically after $\mathrm{t} \simeq 10$ s. The period is 3.46 s, and the angular frequency ω is 1.82 rad/s. Fourier analysis shows that $y_0 \sim y_3$ contains mainly three frequency components of 0, ω, and 2ω. Their amplitudes are 0.36, 0.88, 0.16 in y_1, 0.51, 0.53, 0.12 in y_0, 0.01, 0.05, 0.17 in y_2, and 0.05, 0.09, 0.21 in y_3. The components of ω are dominant in y_1 and y_0 while the components of 2ω are dominant in y_2 and y_3. This synchronization is brought by coupling among the modes.

C. Mode Coupling

With (5), (1) is transformed as follows:

$$\frac{dz}{dt} = \psi(z) \tag{6}$$

where

$$\psi(z) \equiv M^{-1}\varphi(u_o + Mz) \equiv (f_0(z), g_0(z), f_1(z), g_1(z), \ldots)^t.$$

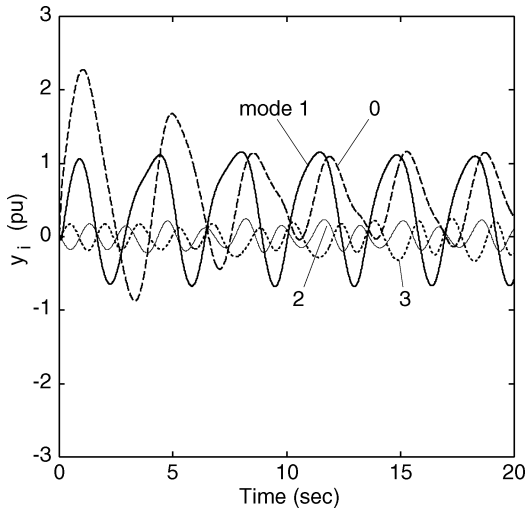

Fig. 6. Mode components.

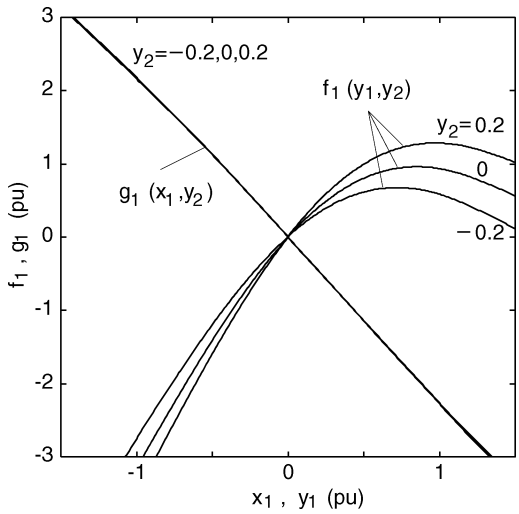

Fig. 7. Effect of mode 2 on mode 1.

Since $\psi(0) = 0$, $z = 0$ is an equilibrium point. f_i, g_i is force which acts on x_i, y_i, respectively. We rewrite $\varphi(u)$ as

$$\varphi(u) = Av + \bar{\varphi}(v) \tag{7}$$

where $\bar{\varphi}(v)$ consists of the second and higher order terms of v. Substituting (7) into (6) yields

$$\frac{dz}{dt} = Jz + \bar{\psi}(z) \tag{8}$$

where

$$J \equiv M^{-1}AM, \quad \bar{\psi}(z) \equiv M^{-1}\bar{\varphi}(Mz).$$

J is a block diagonal matrix

$$J = diag(J_0, J_1, \ldots) \tag{9}$$

where J_i is a 2×2 or 1×1 matrix. For a pair of conjugate eigenvalues $\lambda_i, \bar{\lambda}_i = d_i \pm j\omega_i$, J_i becomes

$$J_i = \begin{pmatrix} d_i & \omega_i \\ -\omega_i & d_i \end{pmatrix}.$$

For a real eigenvalue $\lambda_i = d_i$, J_i reduces to

$$J_i = d_i.$$

If the nonlinear term $\bar{\psi}(z) \equiv 0$ in (8), all modes are decoupled. However, this is not always true.

As an example, we consider mode 1. From (6), f_1 and g_1 are functions of z. To examine coupling with mode 2, we set z as

$$z = (0, 0, 0, y_1, 0, y_2, 0, \ldots, 0)^t$$

and calculate $f_1(z)$, which is denoted by $f_1(y_1, y_2)$. Similarly, we set z as

$$z = (0, 0, x_1, 0, 0, y_2, 0, \ldots, 0)^t$$

and define $g_1(x_1, y_2)$. Fig. 7 shows variations of $f_1(y_1, y_2)$ and $g_1(x_1, y_2)$ with y_1 or x_1, where $y_2 = -0.2$, 0, or 0.2. Clearly, $f_1(0,0) = g_1(0,0) = 0$. If $y_2 = 0$, their inclinations are $\partial f_1/\partial y_1 = \omega_1$ and $\partial g_1/\partial x_1 = -\omega_1$ at the origin. In Fig. 7, the inclination of g_1 changes little with y_2, However, the inclination of f_1 changes considerably with y_2. Hence, f_1 and g_1 are approximated as follows:

$$f_1(y_1, y_2) = (\omega_1 + \beta y_2)y_1, \quad g_1(x_1, y_2) = -\omega_1 x_1.$$

We can examine coupling with x_2 or other modes in a similar manner. However, if other nonlinear terms are negligible, mode 1 varies as

$$\begin{aligned} \frac{dx_1}{dt} &= d_1 x_1 + \omega_1 y_1 + \beta y_1 y_2 \\ \frac{dy_1}{dt} &= -\omega_1 x_1 + d_1 y_1. \end{aligned} \tag{10}$$

If $y_2 = c\sin\omega_2 t$, the inclination of f_1 changes periodically, and if $c\beta$ is large enough, mode 1 diverges even if $d_1 < 0$. This is known as parametric excitation [14], [15]. The instability is conspicuous when $\omega_2 = 2\omega_1$.

IV. Interaction Between Modes

We assume $d_i < 0$ for all i. The equilibrium point $z = 0$ is stable and has a region of attraction. We simply say a system is stable when it converges to $z = 0$. If y_2 reduces to 0 in (10), no instability occurs. Some interaction among modes is necessary to explain the phenomenon in Fig. 4.

Modes $0 \sim 3$ in Fig. 6 play main roles in the phenomenon. In this section, we consider their interaction. Other modes are small in amplitude, and have weak coupling with these modes. They are considered in the next section.

A. Interaction Between Mode 1 and 0

First, we consider interaction between mode 1 and 0. The modes vary according to

$$\begin{aligned} \frac{dx_1}{dt} &= d_1 x_1 + \omega_1 y_1 - \alpha_1 y_1^2 + \beta_0 y_0 y_1 \\ \frac{dy_1}{dt} &= -\omega_1 x_1 + d_1 y_1 \\ \frac{dx_0}{dt} &= d_0 x_0 + \omega_0 y_0 \\ \frac{dy_0}{dt} &= -\omega_0 x_0 + d_0 y_0 + \alpha_0 y_1^2. \end{aligned} \tag{11}$$

Only essential terms are included to simplify analysis. $\beta_0 y_0 y_1$ means that f_1 changes its inclination with y_0. $\alpha_1 y_1^2$ means that f_1 is not a straight line as seen in Fig. 7. g_0 is affected by y_1 through $\alpha_0 y_1^2$.

If $\beta_0 = 0$, mode 1 is independent of mode 0. Its variation is described by the first two equations in (11). The system has a quadratic term $\alpha_1 y_1^2$, and it may have some limit cycles [16]. However, no limit cycle exists in this case as shown in the Appendix. Similary, if $\alpha_0 = 0$, mode 0 is independent of mode 1. It clearly has no limit cycle. The terms $\beta_0 y_0 y_1$ and $\alpha_0 y_1^2$ form main parts in interaction between mode 1 and 0, and they make the system unstable.

For example, we choose the parameters as $d_1 = d_0 = -0.1$, $\omega_1 = 2$ rad/s, $\omega_0 = 1.33$ rad/s, $\alpha_1 = 1$, $\beta_0 = 0.75$, and $\alpha_0 = 0.5$. In Fig. 6, modes 1 and 0 are both excited by the fault. However, to show the importance of mode 1, we set the initial system state as follows:

$$x_1 = 0, \quad y_1 = y_1^0, \quad x_0 = 0, \quad y_0 = 0.$$

The system diverges if y_1^0 is greater than a boundary value. Fig. 8(a) shows an unstable case where y_1^0 is 1.69 while the boundary value is 1.688. Mode 0, initially set zero, is excited by mode 1. Conversely, mode 1, if set zero, is not excited by mode 0 as is clear from (11). The boundary value changes with the intial state. In the next section, we set the initial state by (5) with $v = u - u_0$ at fault clearing time t_c. The boundary value varies with ω_1 as in Fig. 8(b). If we increase damping, the stable region enlarges. Fig. 8(c) shows curves of y_1-f_1 and x_1-g_1 for a boundary case B_1. g_1 draws a simple closed curve due to $d_1 y_1$. However, f_1 twists once, which is brought by $\beta_0 y_0 y_1$. If $d_1 = \beta_0 = 0$, f_1 reduces to

$$f_1(y_1) \equiv \omega_1 y_1 - \alpha_1 y_1^2.$$

In Fig. 8(c), U is a point where $f_1(y_1) = 0$ holds. Over U, $f_1(y_1) < 0$, and mode 1 monotonically diverges. In the boundary case, f_1 starts from the point indicated by B_1, and converges to the closed curve. The value of y_1 at U varies with ω_1, as shown in Fig. 8(b).

Mode 0 is synchronized with mode 1 in Figs. 6 and 8(a) while their natural frequencies are different. This is caused by term $\alpha_0 y_1^2$. Since y_1 varies periodically for the boundary case B_1, we approximate it as

$$y_1 = c_1 + c_2 \cos \omega t \tag{12}$$

where c_1 and c_2 are constants [14]. Substituting

$$y_1^2 = \left(c_1^2 + \frac{1}{2}c_2^2\right) + 2c_1 c_2 \cos \omega t + \frac{1}{2}c_2^2 \cos 2\omega t$$

into (11) gives

$$y_0 \simeq \frac{2\alpha_0 c_1 c_2 \omega}{\omega^2 - \omega_0^2} \sin \omega t + \frac{\alpha_0 c_2^2 \omega}{4\omega^2 - \omega_0^2} \sin 2\omega t \tag{13}$$

where $d_0 \simeq 0$ is assumed. In Fig. 8(c), $c_1 \simeq 0.271$, $c_2 \simeq 1.278$, and $\omega \simeq 1.653$ rad/s, and accordingly $y_0 \simeq 0.566 \sin \omega t + 0.134 \sin 2\omega t$. This explains why y_0 is synchronized with y_1. If $c_1 = 0$, the $\sin \omega t$ term does not appear. By substituting (12) and (13) into the first equation of (11), and examining its coefficients on constant, $\cos \omega t$, and $\sin \omega t$ terms, we obtain

$$c_1 = \frac{\alpha_1}{\omega_1}\left(c_1^2 + \frac{c_2^2}{2}\right) \simeq \frac{\alpha_1}{2\omega_1} c_2^2 \tag{14}$$

$$\omega^2 = \omega_1^2 - 2\omega_1 \alpha_1 c_1 \tag{15}$$

$$0 = d_1 + \alpha_0 \beta_0 \left(\frac{\omega_1}{\omega^2 - \omega_0^2} c_1^2 + \frac{\omega_1}{4\omega^2 - \omega_o^2} \frac{c_2^2}{4}\right). \tag{16}$$

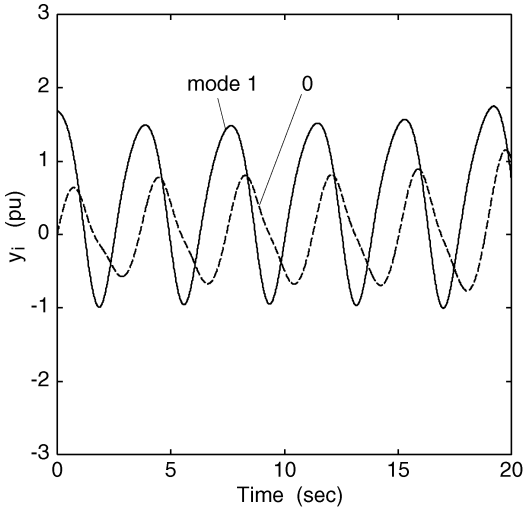

(a)

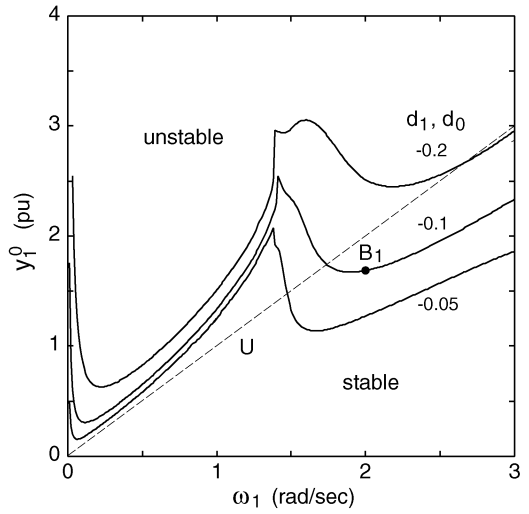

(b)

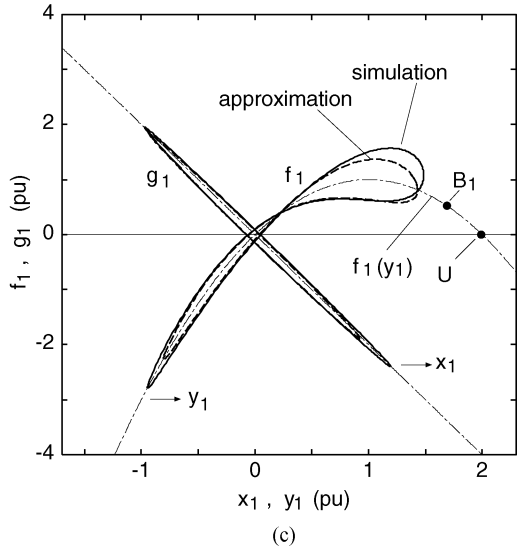

(c)

Fig. 8. Interaction between mode 1 and 0.

The periodic solution y_1 in (12) must satisfy these relations. The constant term c_1 arises owing to $\alpha_1 y_1^2$ as is clear from (14), and it rapidly increases with c_2. The frequency ω lowers with c_1

according to (15). The right side of (16) is related with damping of mode 1. It starts from $d_1 < 0$, increases with c_1 and c_2, and reaches zero, where we obtain periodic oscillations, i.e., a limit cycle. This is shown in Fig. 8(c) by dotted lines, where $c_1 = 0.314$, $c_2 = 1.12$, and $\omega = 1.657$ rad/s.

B. Interaction Among Mode 1, 2, and 3

Interaction between mode 1 and 2 is a crucial factor in the instability of Fig. 4 although it is not so simple as that between mode 1 and 0. Next, we consider a system described as follows:

$$\begin{aligned}
\frac{dx_1}{dt} &= d_1 x_1 + \omega_1 y_1 - \alpha_1 y_1^2 + \beta_1 y_1 y_2 \\
\frac{dy_1}{dt} &= -\omega_1 x_1 + d_1 y_1 \\
\frac{dx_2}{dt} &= d_2 x_2 + \omega_2 y_2 + \beta_2 y_1 y_3 \\
\frac{dy_2}{dt} &= -\omega_2 x_2 + d_2 y_2 \\
\frac{dx_3}{dt} &= d_3 x_3 + \omega_3 y_3 + \alpha_3 y_1^2 - \beta_3 y_1 y_3 \\
\frac{dy_3}{dt} &= -\omega_3 x_3 + d_3 y_3. \qquad (17)
\end{aligned}$$

There are four nonlinear terms besides $\alpha_1 y_1^2$, i.e., $\beta_1 y_1 y_2$, $\beta_2 y_1 y_3$, $\alpha_3 y_1^2$, and $\beta_3 y_1 y_3$. Even if $d_1,\ d_2,\ d_3 < 0$, these terms cause instability.

As an example, we choose the parameters as $d_1 = d_2 = d_3 = -0.1$, $\omega_1 = 2.15$ rad/s, $\omega_2 = 3.94$ rad/s, $\omega_3 = 4.16$ rad/s, $\alpha_1 = 1$, $\alpha_3 = 0.1$ $\beta_1 = 2$, $\beta_2 = 0.5$, and $\beta_3 = 1.5$. The initial system state is

$$x_1 = 0, \quad y_1 = y_1^0, \quad x_2 = y_2 = x_3 = y_3 = 0.$$

The system is unstable if y_1^0 is greater than a boundary value. Fig. 9(a) shows an unstable case, where y_1^0 is 0.204 while the boundary value is 0.2025. The boundary value changes with ω_1 as in Fig. 9(b). When damping is small as $d_1 = d_2 = d_3 = -0.05$, we can see a sharp dip of y_1^0 in the vicinity of $\omega_1 = 2.07$ rad/s, where $\omega_1 \simeq \omega_2/2 \simeq \omega_3/2$ holds. This is due to resonance as described later. If we increase damping, the stable region enlarges. Fig. 9(c) shows curves of y_1-f_1 and x_1-g_1 for a boundary case B_2. Though g_1 draws a simple closed curve, f_1 is twisted at two points, which is caused by periodic change in the inclination of f_1 through the term $\beta_1 y_1 y_2$.

We assume again y_1 varies periodically as

$$y_1 = c_1 + c_2 \cos \omega t. \qquad (18)$$

There is no direct excitation of mode 2 by mode 1. Mode 3 is excited first through the term $\alpha_3 y_1^2$, and then mode 2 is excited through $\beta_2 y_1 y_3$. y_2 is expressed as

$$y_2 = s_1 + s_2 \sin \omega t + s_3 \cos \omega t + s_4 \sin 2\omega t + s_5 \cos 2\omega t + \cdots. \qquad (19)$$

Substituting (18) and (19) into the first equation of (17), and comparing its coefficients on constant, $\cos \omega t$, and $\sin \omega t$ terms yield

$$c_1 = \frac{\omega_1}{\omega_1^2 + d_1^2}\left\{\alpha_1\left(c_1^2 + \frac{c_2^2}{2}\right) - \beta_1\left(c_1 s_1 + \frac{1}{2} c_2 s_3\right)\right\} \qquad (20)$$

$$\omega^2 = \omega_1^2 + d_1^2 - 2\omega_1 \alpha_1 c_1 + \omega_1 \beta_1 \left(\frac{c_1}{c_2} s_3 + s_1 + \frac{1}{2} s_5\right) \qquad (21)$$

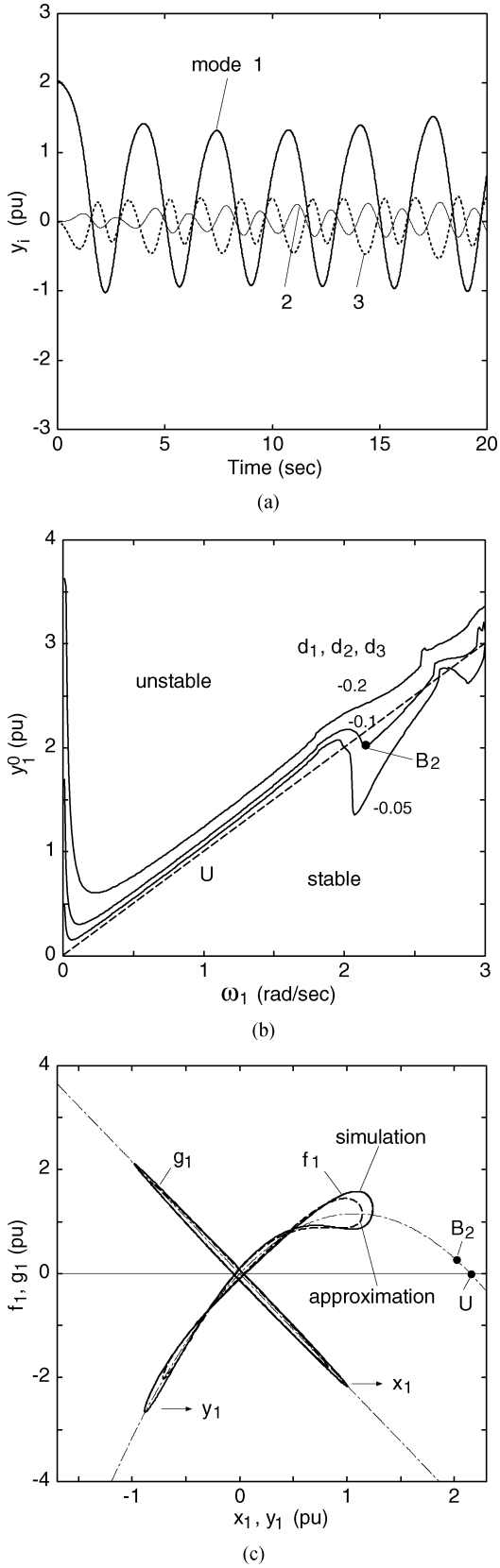

Fig. 9. Interaction among mode 1, 2, and 3.

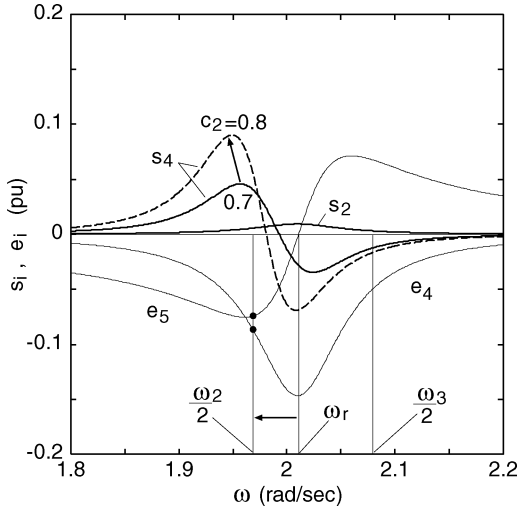

Fig. 10. Coefficients of y_2 and y_3.

$$0 = d_1 + \frac{\omega_1\beta_1}{2\omega}\left(\frac{c_1}{c_2}s_2 + \frac{1}{2}s_4\right). \tag{22}$$

For derivation, refer to the Appendix . These equations must be satisfied by c_1, c_2, and ω for a periodic solution y_1 in (18) to exist. We calculate c_1 and ω from (20) and (21) for a given value of c_2, and then examine whether (22) holds or not. Since its second term increases with c_2, (22) is satisfied for some value of c_2.

Fig. 10 shows variation of s_2 and s_4 in (19), where $c_2 = 0.7$. Since s_2 is small compared with s_4, we examine s_4 further. By expressing $\beta_2 y_1 y_3$ as

$$\beta_2 y_1 y_3 = h_1 + h_2\sin\omega t + h_3\cos\omega t + h_4\sin 2\omega t + h_5\cos 2\omega t + \cdots \tag{23}$$

we obtain

$$s_4 = \omega_2\frac{(4\omega^2 - \omega_2^2 - d_2^2)h_4 + 4\omega d_2 h_5}{(4\omega^2 - \omega_2^2 - d_2^2)^2 + 16\omega^2 d_2^2}.$$

s_4 takes large values in the vicinity of

$$\omega = \frac{1}{2}\sqrt{\omega_2^2 + d_2^2} \simeq \frac{\omega_2}{2}.$$

Similarly, by expressing y_3 as

$$y_3 = e_1 + e_2\sin\omega t + e_3\cos\omega t + e_4\sin 2\omega t + e_5\cos 2\omega t \tag{24}$$

we obtain

$$h_4 = \beta_2\left(c_1 e_4 + \frac{1}{2}c_2 e_2\right), \quad h_5 = \beta_2\left(c_1 e_5 + \frac{1}{2}c_2 e_3\right).$$

Fig. 10 shows e_4 and e_5, too. Neglecting $e_1 \sim e_3$ gives

$$e_4 = \frac{4\omega d_3\omega_3}{(4\omega^2 - \omega_3^2 - d_3^2 + \omega_3\beta_3 c_1)^2 + 16\omega^2 d_3^2} \times \frac{1}{2}\alpha_3 c_2^2$$
$$e_5 = \frac{(4\omega^2 - \omega_3^2 - d_3^2 + \omega_3\beta_3 c_1)\omega_3}{(4\omega^2 - \omega_3^2 - d_3^2 + \omega_3\beta_3 c_1)^2 + 16\omega^2 d_3^2} \times \frac{1}{2}\alpha_3 c_2^2.$$

They take large values in the neighborhood of

$$\omega = \omega_r \simeq \frac{1}{2}\sqrt{\omega_3^2 + d_3^2 - \omega_3\beta_3 c_1}.$$

With an increase in c_2 and c_1, ω_r approaches $\omega_2/2$ to make e_4, e_5, and s_4 large. As a result, (22) holds when $c_2 = 0.93$. Fig. 9(c) shows an approximate result obtained by (18)~(22), where $c_1 = 0.214$ and $\omega = 1.921$ rad/s.

C. Interaction Among Mode 1, 0, 2, and 3

Two systems described by (11) and (17) become unstable due to nonlinear interaction among modes. Lastly, we combine them as follows:

$$\begin{aligned}
\frac{dx_0}{dt} &= d_0 x_0 + \omega_0 y_0 - \gamma_1 y_1^2 + \gamma_2 y_1^4 + \gamma_3 y_0 y_1 \\
\frac{dy_0}{dt} &= -\omega_0 x_0 + d_0 y_0 + \alpha_0 y_1^2 \\
\frac{dx_1}{dt} &= d_1 x_1 + \omega_1 y_1 - \alpha_1 y_1^2 + \beta_0 y_0 y_1 + \beta_1 y_1 y_2 - \gamma_4 y_1 y_3 \\
\frac{dy_1}{dt} &= -\omega_1 x_1 + d_1 y_1 \\
\frac{dx_2}{dt} &= d_2 x_2 + \omega_2 y_2 + \beta_2 y_1 y_3 + \gamma_5 y_1^2 - \gamma_6 y_1 y_0 \\
\frac{dy_2}{dt} &= -\omega_2 x_2 + d_2 y_2 \\
\frac{dx_3}{dt} &= d_3 x_3 + \omega_3 y_3 + \alpha_3 y_1^2 - \beta_3 y_1 y_3 \\
\frac{dy_3}{dt} &= -\omega_3 x_3 + d_3 y_3.
\end{aligned} \tag{25}$$

Nonlinear terms like $\alpha_0 y_1^2, \alpha_1 y_1^2, \beta_0 y_0 y_1, \ldots$ are included in the system. These terms are essential to this system. Some other terms with coefficients $\gamma_1 \sim \gamma_6$ are also included. They have small, but some influence as a whole.

We choose parameters as follows: $\omega_0 = 1.330, d_0 = -0.287$, $\omega_1 = 2.272$, $d_1 = -0.164$, $\omega_2 = 3.937$, $d_2 = -0.037$, $\omega_3 = 4.159$, $d_3 = -0.044$, $\alpha_0 = 0.579$, $\alpha_1 = 1.254$, $\alpha_3 = 0.098$, $\beta_0 = 0.747, \beta_1 = 1.907, \beta_2 = 0.506, \beta_3 = 1.253, \gamma_1 = 1.301$, $\gamma_2 = 0.152, \gamma_3 = 0.881, \gamma_4 = 0.543, \gamma_5 = 0.059, \gamma_6 = 0.059$. These values apply to the system of Fig. 4. The initial system state is set as

$$x_0 = y_0 = x_1 = 0, \quad y_1 = y_1^0, \quad x_2 = y_2 = x_3 = y_3 = 0.$$

Fig. 11(a) shows the boundary value of y_1^0. It varies with ω_1. Fig. 11(b) shows time variations of y_0, y_1, y_2, and y_3 for a boundary case B_3. We can see variation similar to Fig. 6. Fig. 11(c) shows curves of $y_1 - f_1$ and $x_1 - g_1$ for the same case. g_1 draws a simple closed curve, and f_1 is twisted at two points. This is similar to Fig. 9(c).

We rewrite the third equation of (25) as follows:

$$\frac{dx_1}{dt} = d_1 x_1 + \omega_1 y_1 - \alpha_1 y_1^2 + \beta_1 y_1 \tilde{y}_2 \tag{26}$$

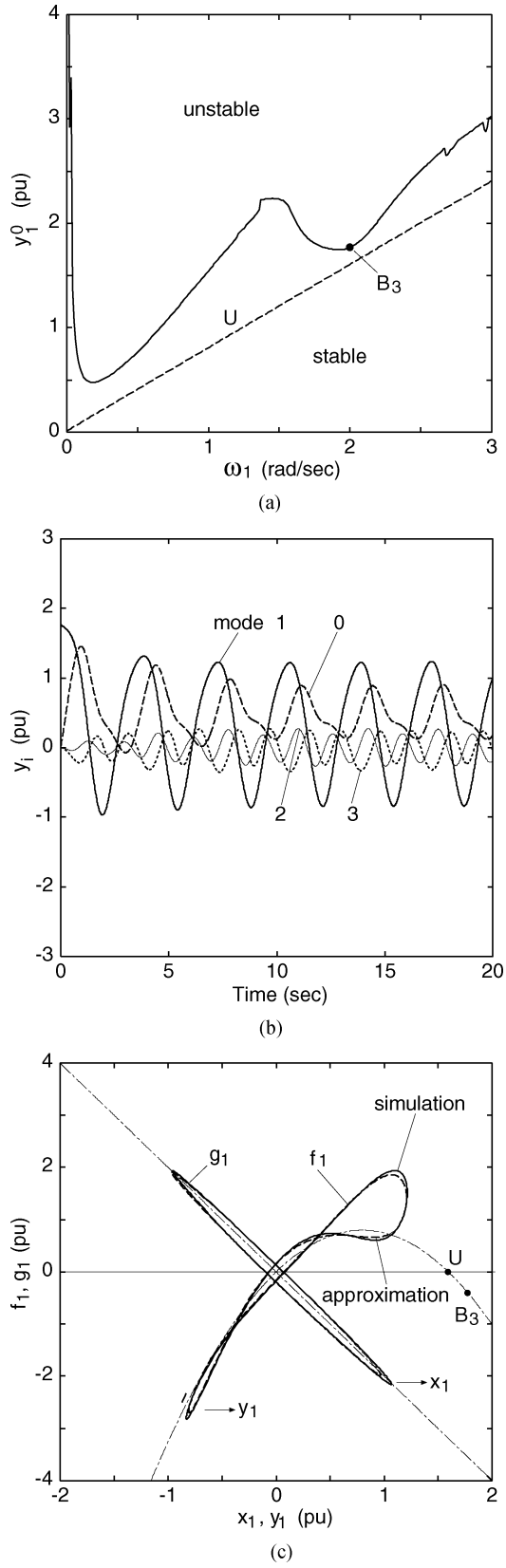

Fig. 11. Interaction among mode 1, 0, 2, and 3.

where

$$\tilde{y}_2 = y_2 + \frac{(\beta_0 y_0 - \gamma_4 y_3)}{\beta_1}.$$

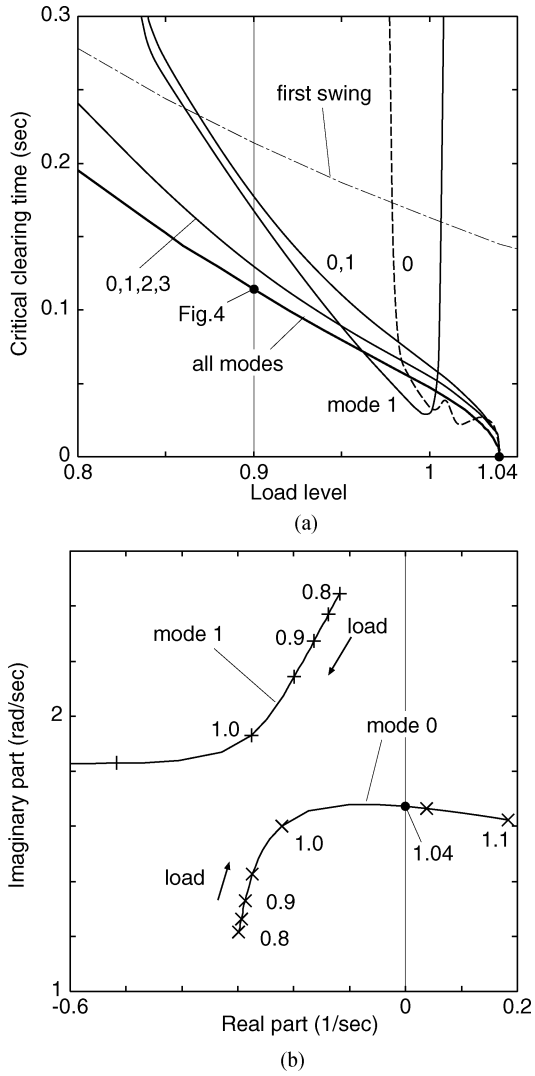

Fig. 12. Detailed analysis.

Equation (26) is similar to one in (17). Considering (13) and (24), we represent $\tilde{y}_2$ as (19), then (20)~(22) follow. As a trial, we approximate as

$$\begin{aligned} y_1 &= 0.20 + 1.01\cos\omega t \\ \tilde{y}_2 &= 0.17 + 0.13\sin\omega t + 0.10\cos\omega t \\ &\quad + 0.28\sin 2\omega t + 0.08\cos 2\omega t \end{aligned}$$

where $\omega = 1.916\ \mathrm{rad/s}$. With these approximations, we obtain broken lines in Fig. 11(c). Since the $\sin 2\omega t$ term is large, f_1 is twisted at two points. If we neglect this term, f_1 twists at one point due to the $\sin\omega t$ term as in Fig. 8(c). We substitute $s_2 = 0.13$ and $s_4 = 0.28$ into the right side of (22). Its value becomes 0.001, and (22) is accurately satisfied.

V. Detailed Analysis

Equations (16) and (22) shows that the stability of mode 1 is affected by interaction with other modes. To understand its mechanism, we used simple models as (11), (17), and (25). In this section, we use more accurate models based on (6). For

example, when considering interaction between mode 1 and 0, we set z as

$$z = (x_0, y_0, x_1, y_1, 0, \ldots, 0)^t$$

and numerically integrate (6). The initial value of z is calculated by (5) from u at clearing time t_c. We can arbitrarily increase the number of modes to consider in the same way.

Fig. 12(a) shows variation of critical clearing time. If all modes are considered, its value coincides with that obtained by (1). The critical clearing time is small compared with that for the first swing instability. It reduces to zero at load level 1.04, where the eigenvalue of mode 0 crosses the imaginary axis after passing near a strong resonance [17] with mode 1 as in Fig. 12(b). In this range, mode 0 is weakly damped. It has an unstable limit cycle by itself for load > 1.026, and causes a subcritical Hopf bifurcation at load 1.04. However, our interest is in the load level ≤ 1 where mode 1 forms an unstable limit cycle through interaction with other modes. We examine it further.

First, we consider mode 1 alone. In this case, mode 1 monotonically diverges if it crosses the point U shown in Fig. 8(b) and (c). By combining with mode 0, the critical clearing time improves a little. However, mode 1 diverges in an oscillatory manner as seen in Fig. 8(a). If we add mode 2 and 3 further, the critical clearing time deteriorates. Its value is close to that obtained by incorporating all modes. We can confirm that mode 0, 2, and 3 have significant influence on the stability of mode 1. In practical systems, critical clearing times are kept greater than 0.1 s. Under such operating conditions, this mode interaction is thought to play important role.

VI. Conclusions

In this paper, we considered an instability of a low-frequency interarea mode in the IEEJ West 30-machine system model. The results are summarized as follows.

1) The interarea mode (mode 1) is stable for small disturbances, but diverges in an oscillatory manner for large ones. Its critical clearing time is considerably small compared with that for the first swing instability.
2) Mode 1 is stable by itself, but diverges owing to interaction with other modes.
3) Mode 0 is related with control systems. Its natural frequency is lower than mode 1. It is excited by mode 1, and acts so as to make mode 1 diverge.
4) Mode 2 is indirectly excited by mode 1 through mode 3. Its natural frequency is two times higher than mode 1. It deteriorates the stability of mode 1 further.
5) All modes must be considered to obtain accurate results, but close results are obtained by considering several main modes.

Appendix

A. Non-Existence of Limit Cycle

If $\beta_0 = 0$, the first two equations in (11) are transformed as follows:

$$\frac{dy_1}{dt} = w(\equiv -\omega_1 x_1 + d_1 y_1)$$
$$\frac{dw}{dt} = 2d_1 w - p y_1 + q y_1^2$$

where $p = \omega_1^2 + d_1^2$, $q = \omega_1 \alpha_1$. There are two equilibrium points in this system, i.e., $y_1 = 0, w = 0$ and $y_1 = p/q, w = 0$. We define a function

$$V = \int_0^w w dw + \int_0^{y_1} (p y_1 - q y_1^2) dy_1 = \frac{1}{2} w^2 + \frac{1}{2} p y_1^2 - \frac{1}{3} q y_1^3.$$

The time derivative of V is

$$\begin{aligned} \frac{dV}{dt} &= w \frac{dw}{dt} + (p y_1 - q y_1^2) \frac{dy_1}{dt} \\ &= w(2d_1 w - p y_1 + q y_1^2) + (p y_1 - q y_1^2) w \\ &= 2 d_1 w^2 \leq 0. \end{aligned} \tag{27}$$

If there is a limit cycle, w and y_1 periodically vary, and V also varies periodically. However, (27) shows that V decreases with time. This contradicts that a limit cycle exists.

B. Derivation of (20)~(22)

From the second equation of (17)

$$\omega_1 x_1 = d_1 y_1 - \frac{dy_1}{dt} = d_1(c_1 + c_2 \cos \omega t) + \omega c_2 \sin \omega t \tag{28}$$

is obtained. Differentiating this equation yields

$$\omega_1 \frac{dx_1}{dt} = -\omega d_1 c_2 \sin \omega t + \omega^2 c_2 \cos \omega t. \tag{29}$$

Substituting (18), (19), and (28) into the first equation of (17) gives

$$\begin{aligned} \omega_1 \frac{dx_1}{dt} = {} & d_1 \{ d_1(c_1 + c_2 \cos \omega t) + \omega c_2 \sin \omega t \} \\ & + \omega_1^2 (c_1 + c_2 \cos \omega t) \\ & + \omega_1 \beta_1 \left\{ \left(c_1 s_1 + \frac{c_2 s_3}{2} \right) + \left(c_1 s_2 + \frac{c_2 s_4}{2} \right) \sin \omega t \right. \\ & \left. + \left(c_1 s_3 + c_2 s_1 + \frac{c_2 s_5}{2} \right) \cos \omega t + \cdots \right\} \\ & - \omega_1 \alpha_1 \left\{ \left(c_1^2 + \frac{c_2^2}{2} \right) + 2 c_1 c_2 \cos \omega t + \frac{c_2^2}{2} \cos 2\omega t \right\}. \end{aligned} \tag{30}$$

By comparing constant, $\cos\omega t$, and $\sin\omega t$ terms in (29) and (30), we obtain

$$\begin{aligned} 0 &= d_1^2 c_1 + \omega_1^2 c_1 + \omega_1\beta_1\left(c_1 s_1 + \frac{c_2 s_3}{2}\right) \\ &\quad - \omega_1\alpha_1\left(c_1^2 + \frac{c_2^2}{2}\right) \\ \omega^2 c_2 &= d_1^2 c_2 + \omega_1^2 c_2 + \omega_1\beta_1\left(c_1 s_3 + c_2 s_1 + \frac{c_2 s_5}{2}\right) \\ &\quad - 2\omega_1\alpha_1 c_1 c_2 \\ -d_1\omega c_2 &= d_1\omega c_2 + \omega_1\beta_1\left(c_1 s_2 + \frac{c_2 s_4}{2}\right). \end{aligned}$$

After some manipulation, (20)–(22) are derived.

ACKNOWLEDGMENT

The authors would like to acknowledge the suggestions of professor T. Takuma in their study. They used LAPACK softwares for the modal analysis in Sections III and V. For the package, refer to http://www.netlib.org.

REFERENCES

[1] Y. Tamura and N. Yorino, "Possibility of auto-& hetero-parametric resonances in power systems and their relationship with long-term dynamics," *IEEE Trans. Power Syst.*, vol. PWRS-2, pp. 890–897, Nov. 1987.

[2] N. Yorino, H. Sasaki, Y. Tamura, and R. Yokoyama, "A generalized analysis method of auto-parametric resonances in power systems," *IEEE Trans. Power Syst.*, vol. 4, pp. 1057–1064, Aug. 1989.

[3] V. Vittal, N. Bhatia, and A. A. Fouad, "Analysis of the inter-area mode phenomenon in power systems following large disturbances," *IEEE Trans. Power Syst.*, vol. 6, pp. 1515–1521, Nov. 1991.

[4] C. M. Lin, V. Vittal, W. Kliemann, and A. A. Fouad, "Investigation of modal interaction and its effects on control performance in stressed power systems using normal forms of vector fields," *IEEE Trans. Power Systems*, vol. 11, pp. 781–787, May 1996.

[5] A. H. Nayfeh and B. Balachandran, "Modal interactions in dynamical and structural systems," *Appl. Mech. Rev.*, pt. 2, vol. 42, no. 11, pp. S175–S201, 1989.

[6] N. Kakimoto, "Instability of low-frequency oscillation in longitudinal power system due to autoparametric resonance," *Trans. Inst. Elect. Eng. Jpn.*, vol. 115-B, no. 3, pp. 219–226, 1995.

[7] N. Kakimoto, T. Mizuguchi, and H. Sugihara, "Physical cause of autoparametric resonance in longitudinal power system," *Trans. Inst. Elect. Eng. Jpn.*, vol. 116-B, no. 2, pp. 140–146, 1996.

[8] N. Kakimoto and M. Nakamura, "Stable region for autoparametric resonance in longitudinal power systems," *Trans. Inst. Elect. Eng. Jpn.*, vol. 118-B, no. 2, pp. 119–126, 1998.

[9] N. Kakimoto and K. Tomiyama, "Verification of autoparametric resonance in longitudinal power system," *Trans. Inst. Elect. Eng. Jpn.*, vol. 119-B, no. 4, pp. 516–523, 1999.

[10] E. H. Abed and P. P. Varaiya, "Nonlinear oscillations in power systems," *Int. J. Elect. Power Energy Syst.*, vol. 6, no. 1, pp. 37–43, 1984.

[11] C. D. Vournas, M. A. Pai, and P. W. Sauer, "The effect of automatic voltage regulation on the bifurcation evolution in power systems," *IEEE Trans. Power Syst.*, vol. 11, pp. 1683–1688, Nov. 1996.

[12] K. Kawasaki, P. Miao, T. Imamura, Y. Mitani, and K. Tsuji, "A method for analysis of dynamics in generator swing based on nonlinear system theory," *Trans. Inst. Elect. Eng. Jpn.*, vol. 120-B, no. 3, pp. 325–332, 2000.

[13] H. Amano, T. Kumano, T. Inoue, and H. Taniguchi, "A stability criterion for nonlinear oscillations in power systems by Hopf bifurcation theory," *Trans. Inst. Elect. Eng. Jpn.*, vol. 121-B, no. 6, pp. 708–714, 2001.

[14] C. Hayashi, *Nonlinear Oscillations in Physical Systems*. New York: McGraw-Hill, 1964.

[15] D. E. Newland, *Mechanical Vibration Analysis and Computation*. White Plains, NY: Longman, 1989.

[16] J. W. Reyn, "Non-existence of limit cycles for a quadratic system in class II," *Nonlin. Anal.*, vol. 50, pp. 323–331, 2002.

[17] I. Dobson, J. Zhang, S. Greene, H. Engdahl, and P. W. Sauer, "Is strong modal resonance a precursor to power system oscillations?," *IEEE Trans. Circuits Syst. I*, vol. 48, pp. 340—349, Mar. 2001.

Naoto Kakimoto (M'78) was born in Japan in 1952. He received the Ph.D. degree in electrical engineering from Kyoto University, Kyoto, Japan, in 1982.

He is presently an Associate Professor at Kyoto University. His research interests are power system stabilities.

Akira Nakanishi was born in Japan in 1977. He received the M.S. degree in electrical engineering in 2001 from Kyoto University, Kyoto, Japan, where he studied autoparametric resonance in power systems.

He is presently with Ito-chu Corporation, Tokyo, Japan.

Mr. Nakanishi is a member of the IEE of Japan.

Katsuyuki Tomiyama was born in Japan in 1945. He received the Ph.D. degree in electrical engineering from Kyoto University, Kyoto, Japan, in 2000.

He is a Chief Researcher at Kansai Electric Power Company, Osaka, Japan.

Mr. Tomiyama is a member of the IEE of Japan.